

## One-Step Synthesis of Au@Pd Core–Shell Nanooctahedron

Young Wook Lee,<sup>†,‡</sup> Minjung Kim,<sup>†,‡</sup> Zee Hwan Kim,<sup>§</sup> and Sang Woo Han<sup>\*,†</sup>

Department of Chemistry and KI for the NanoCentury, KAIST, Daejeon 305-701, Korea, Environmental Biotechnology National Core Research Center, Gyeongsang National University, Jinju 660-701, Korea, and Department of Chemistry, Korea University, Seoul 136-701, Korea

Received July 7, 2009; E-mail: sangwoohan@kaist.ac.kr

Bimetallic nanoparticles are attractive materials owing to their novel optical, catalytic, electronic, and magnetic properties which are distinctly different from those of their monometallic counterparts.<sup>1</sup> As in the case of monometallic nanoparticles, these properties can be controlled by tuning the size and shape of the nanoparticles. Accordingly, bimetallic nanoparticles (core–shell and alloy) with a well-controlled morphology may even show optimized physico-chemical properties.<sup>2</sup> In general, bimetallic nanoparticles have been prepared by simultaneous or successive reduction of metallic precursors. Very recently, a number of bimetallic core–shell nanoparticles with well-defined geometries have been investigated through conformal epitaxial growth of the second metal over the presynthesized seed nanoparticles.<sup>3</sup> However, rationally designed bimetallic heterostructures could not be easily prepared without seeds. Usually, one-pot synthesis such as simultaneous reduction of metallic precursors in the same reaction medium produced a bimetallic alloy or sometimes core–shell particles with uncontrolled spherical shapes.<sup>1,4</sup>

Herein, we report for the first time on the one-step aqueous synthesis of bimetallic core–shell Au–Pd nanoparticles with a well-defined octahedral shape. Among the various bimetallic nanoparticles, Au–Pd nanoparticles have been the subject of intense research due to their efficient catalytic properties for a variety of reactions such as acetylene hydrogenation,<sup>5</sup> H<sub>2</sub>O<sub>2</sub> synthesis,<sup>6</sup> vinyl acetate synthesis,<sup>7</sup> and oxidation of alcohols to aldehydes.<sup>8</sup> Although there have been numerous reports on the synthesis and characterization of Au–Pd nanoparticles, the preparation of particles with well-defined shapes and a controlled atomic distribution is still required to optimize their properties.<sup>9,10</sup>

In this work, precursors of Au and Pd are simultaneously reduced by cetyltrimethylammonium chloride (CTAC) to produce octahedral Au@Pd nanoparticles. In a typical synthesis of Au@Pd core–shell nanoparticles, an aqueous solution of HAuCl<sub>4</sub>/K<sub>2</sub>PdCl<sub>4</sub> mixtures in a molar ratio of 1/1 was added to an aqueous solution of CTAC. This solution was then heated at ~90 °C for ~48 h in an oven. Figure 1a shows a representative SEM image of the prepared sample which demonstrates that the majority of the sample consisted of octahedral nanoparticles with a mean edge length of 41.1 ± 3.5 nm. A high-resolution TEM (HRTEM) image confirms the successful preparation of the core–shell nanostructure (Figure 1b). The average shell thickness was measured to be 5.6 ± 0.8 nm. The high-angle annular dark-field scanning TEM (HAADF-STEM) image and the line profiles of the composition on a single octahedral particle show that the core–shell nanostructure consists of the Au nanooctahedron as a core and a complete shell of Pd (Figure 1d). Elemental mapping of Au and Pd (Figure 1e) also reveals the Au@Pd core–shell structure. A high-magnification HRTEM image

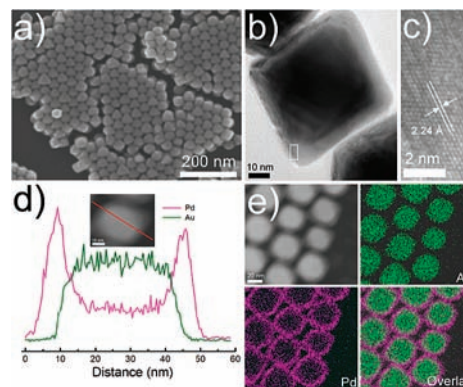


**Figure 1.** (a) SEM and (b) HRTEM images of the Au@Pd nanooctahedra. (c) High-magnification HRTEM image of the square region in (b). (d) HAADF-STEM image and cross-sectional compositional line profiles of an Au@Pd nanooctahedron. (e) HAADF-STEM-EDS mapping images of the Au@Pd nanooctahedra.

of the Au@Pd particle (Figure 1c) reveals the continuous lattice fringes from the Au core to the Pd shell. A *d*-spacing of 2.24 Å for adjacent fringes in the Pd shell region corresponds to the {111} planes of face-centered cubic (fcc) Pd.<sup>9</sup> Selected area electron diffraction and X-ray diffraction patterns recorded on the particles also show the crystalline nature of the prepared particles (Figures S1,2). These results indicate that the Pd shell has been formed through the epitaxial growth of Pd on the Au core. It has been reported that the conformal epitaxial growth of the Pd layer on Au and Pt surfaces could occur when the layer growth rate was adequately low.<sup>3a,d</sup> Different molar ratios of Au and Pd precursors also lead to the formation of octahedral Au@Pd nanoparticles with different sizes of Au cores (Figure S3). The nanoparticles synthesized by using pure Au and pure Pd precursors have octahedral and roughly spherical shapes, respectively, indicating the contribution of epitaxial growth to the shape control of bimetallic particles (Figure S4).

In our experiment, CTAC was used as both a reductant and stabilizer. Recently, it has been found that some ammonium molecules such as poly(diallyl dimethylammonium) chloride<sup>11</sup> and cetyltrimethylammonium bromide (CTAB)<sup>12</sup> have a reducing capacity in hydrothermal synthesis conditions. In fact, comparison of FT-IR spectra between original CTAC and CTAC-stabilized Au@Pd nanoparticles reveals that the nitroso group has been produced after reaction through the oxidation of CTAC (Figure S5 and Table S1). Due to the weak reducing power of CTAC under our synthetic conditions, the reduction rate of metal precursors was very slow, however. The slow reduction kinetics may also be related to the presence of oxygen in this closed system, which may slowly dissolve the reduced metal atoms.<sup>13</sup> Based on the reduction potentials of Au(III) and Pd(II) (Au<sup>3+</sup> (AuCl<sub>4</sub><sup>-</sup>/Au, +1.002 V vs

<sup>†</sup> KAIST.

<sup>‡</sup> Gyeongsang National University.

<sup>§</sup> Korea University.

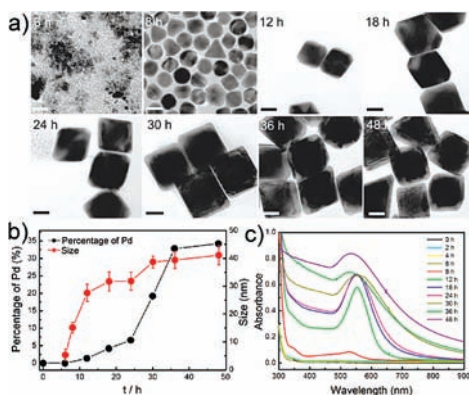


**Figure 2.** (a) TEM images of nanoparticles collected at different reaction times. The scale bars are 20 nm. (b) Changes in the size and mole % of Pd of the particles during the reaction estimated from TEM and ICP-MS analyses, respectively. (c) UV-vis spectra of reaction solution reacted under different reaction times.

SHE (standard hydrogen electrode)) and  $\text{Pd}^{2+}$  ( $\text{PdCl}_4^{2-}/\text{Pd}$ , +0.591 V vs SHE),<sup>14</sup> we can easily expect that Au(III) will be preferentially reduced over the Pd(II) under our experimental conditions. Therefore, the formation of the core-shell particles is likely to be initiated by nucleation of Au atoms to form the Au octahedral core which subsequently acts as a nucleic center for the growth of the Pd layer. The monitoring of the evolution process shown in Figure 2 indeed confirms our hypothesis. As shown by TEM and inductively coupled plasma mass spectrometry (ICP-MS) analyses (Figure 2a,b), small Au octahedral particles were formed initially and grew in size. After  $\sim 18$  h, the size of the Au particle was barely changed and Pd became deposited onto the surfaces of Au cores up to 36 h. Beyond 36 h, no significant change in either the structure or composition was observed. Changes of the Pd shell thickness during the reaction indicate that the shell thickness can be controlled via different reaction times (Figure S6). The structural evolution also accompanied distinct changes in the UV-vis spectral features of the reaction mixtures. Figure 2c shows the extinction spectra of the reaction solution obtained at different reaction times. When the reaction time was increased to 8 h, the single surface plasmon resonance (SPR) peak appeared, which can be assigned to the dipole resonance of octahedral Au core,<sup>15</sup> and the intensity of the peak increased until 18 h. By further increasing the reaction time, the SPR peak of Au core was gradually damped. As is previously reported,<sup>16</sup> shells of Pd or Pt strongly damp out the dipolar plasmon oscillations of Au or Ag cores, because Pd or Pt have significantly lower conductivities at optical frequency than those of Au or Ag. As such, an increase in shell thickness progressively damps out the SPR peak of the core. The observed spectral changes were also reflected in the color change of the solution during the reaction (Figure S7). Both the electron microscopy and spectroscopy data clearly confirm that the core-shell nanoparticles are formed via the sequential formation of the Au core followed by the Pd layer.

We believe that the temporal separation of the formation of the Au octahedron from the formation of the Pd layer owing to the slow reduction kinetics is the key to the formation of the core-shell structure. This was confirmed by the fact that an analogous experiment with a stronger reductant, such as ascorbic acid, resulted in homogeneously alloyed Au-Pd nanoparticles (Figure S8). The shape of noble metal nanoparticles can be modulated by controlling the relative growth rate on particular crystallographic surfaces during the crystal growth through the specific adsorption of surfactants, stabilizers, and ions as well as by controlling the reduction kinetics

of metal precursors.<sup>17</sup> In this regard, CTAC used in the present study as a surfactant molecule plays a critical role in the formation of octahedral nanoparticles. When CTAC was substituted by CTAB which has been commonly used in the shape-controlled synthesis of metal nanoparticles, octahedral particles were not produced; instead, a mixture of particles with a variety of shapes was formed (Figure S9). This can be attributed to the presence of a bromide ion. Bromide can chemisorb onto the surface of seeds more strongly than chloride and thus alter the order of surface free energy, resulting in the promotion of the formation of less stable facets such as {100} and {110}.<sup>18</sup>

In summary, we have presented a simple one-pot synthesis method for the production of octahedral core-shell nanoparticles. Such core-shell nanoparticles with well-defined shapes can be used as a new platform for studying physicochemical properties of nanostructured nanomaterials and will find a number of optical and catalytic applications. For instance, the prepared nanoparticles exhibit efficient surface-enhanced Raman scattering (SERS) properties (Figures S10,11). Given the distinct chemical nature of Pd-coating of the Au@Pd nanooctahedron, together with its SERS activity, *in situ* spectroscopic characterization of catalytic reactions could be possible by using the present system.

**Acknowledgment.** This work was supported by the Basic Science Research Program through the NRF funded by the Korean government (MEST) (R15-2003-012-01001-0, R11-2008-052-02003). Z.H.K. acknowledges the support by the NRF grant (No. R11-2008-095-01000-0) funded by the MEST.

**Supporting Information Available:** Experimental details, Figures S1–S11, and Table S1. This material is available free of charge via the Internet at <http://pubs.acs.org>.

## References

- (1) Toshima, N.; Yonezawa, T. *New J. Chem.* **1998**, *22*, 1179.
- (2) Tao, F.; Grass, M. E.; Zhang, Y.; Butcher, D. R.; Renzas, J. R.; Liu, Z.; Chung, J. Y.; Mun, B. S.; Salmeron, M.; Somorjai, G. A. *Science* **2008**, *322*, 932.
- (3) (a) Habas, S. E.; Lee, H.; Radmilovic, V.; Somorjai, G. A.; Yang, P. *Nat. Mater.* **2007**, *6*, 692. (b) Lim, B.; Wang, J.; Camargo, P. H. C.; Jiang, M.; Kim, M. J.; Xia, Y. *Nano Lett.* **2008**, *8*, 2535. (c) Fan, F.-R.; Liu, D.-Y.; Wu, Y.-F.; Duan, S.; Xie, Z.-X.; Jiang, Z.-Y.; Tian, Z.-Q. *J. Am. Chem. Soc.* **2008**, *130*, 6949.
- (4) (a) Ferrer, D.; Torres-Castro, A.; Gao, X.; Sepúlveda-Guzmán, S.; Ortiz-Méndez, U.; José-Yacamán, M. *Nano Lett.* **2007**, *7*, 1701. (b) Chen, C.-H.; Sarma, L. S.; Chen, J.-M.; Shih, S.-C.; Wang, G.-R.; Liu, D.-G.; Tang, M.-T.; Lee, J.-F.; Hwang, B.-J. *ACS Nano* **2007**, *1*, 114.
- (5) Choudhary, T. V.; Sivadinarayana, C.; Datye, A. K.; Kumar, D.; Goodman, D. W. *Catal. Lett.* **2003**, *86*, 1.
- (6) Edwards, J. K.; Solsona, B.; Landon, P.; Carley, A. F.; Herzing, A.; Watanabe, M.; Kiely, C. J.; Hutchings, G. J. *J. Mater. Chem.* **2005**, *15*, 4595.
- (7) Chen, M.; Kumar, D.; Yi, C.-W.; Goodman, D. W. *Science* **2005**, *310*, 291.
- (8) Enache, D. I.; Edwards, J. K.; Landon, P.; Solsona-Espriu, B.; Carley, A. F.; Herzing, A. A.; Watanabe, M.; Kiely, C. J.; Knight, D. W.; Hutchings, G. J. *Science* **2006**, *311*, 362.
- (9) Lee, Y. W.; Kim, N. H.; Lee, K. Y.; Kwon, K.; Kim, M.; Han, S. W. *J. Phys. Chem. C* **2008**, *112*, 6717.
- (10) Huang, X.; Zheng, N. *J. Am. Chem. Soc.* **2009**, *131*, 4602.
- (11) Chen, H.; Wang, Y.; Dong, S. *Inorg. Chem.* **2007**, *46*, 10587.
- (12) Chen, Y.; Zhang, Y.; Yao, Q.-Z.; Zhou, G.-T.; Fu, S.; Fan, H. *J. Solid State Chem.* **2007**, *180*, 1218.
- (13) Chang, C.-C.; Wu, H.-L.; Kuo, C.-H.; Huang, M. H. *Chem. Mater.* **2008**, *20*, 7570.
- (14) Lee, K. Y.; Kim, M.; Lee, Y. W.; Lee, J.-J.; Han, S. W. *Chem. Phys. Lett.* **2007**, *440*, 249.
- (15) Heo, J.; Kim, D.-S.; Kim, Z. H.; Lee, Y. W.; Kim, D.; Kim, M.; Kwon, K.; Park, H. J.; Yun, W. S.; Han, S. W. *Chem. Commun.* **2008**, 6120.
- (16) Tian, Z.-Q.; Ren, B.; Li, J.-F.; Yang, Z.-L. *Chem. Commun.* **2007**, 3514.
- (17) Jeong, G. H.; Kim, M.; Lee, Y. W.; Choi, W.; Oh, W. T.; Park, Q.-H.; Han, S. W. *J. Am. Chem. Soc.* **2009**, *131*, 1672.
- (18) Xiong, Y.; Cai, H.; Wiley, B. J.; Wang, J.; Kim, M. J.; Xia, Y. *J. Am. Chem. Soc.* **2007**, *129*, 3665.

JA905603P